

Computational Screening of Ligands for Enhanced Interactions between Lead Halide Perovskite Quantum Dots

Elizabeth Stippell,¹ Carlos Mora-Perez,¹ Nicholas Favate,² Libai Huang,² Christina W. Li,²
Oleg V. Prezhdo^{1,3,*}

¹*Department of Chemistry, University of Southern California, Los Angeles, CA 90089*

²*Department of Chemistry, Purdue University, West Lafayette, IN 47907, USA*

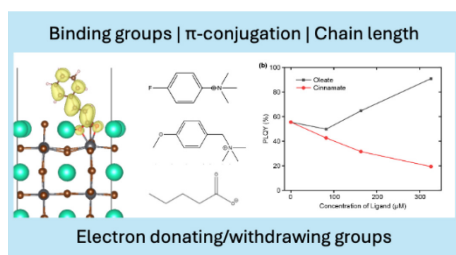
³*Department of Physics and Astronomy, University of Southern California, Los Angeles, CA 90089*

Abstract.

Ligand choice in nanoparticle systems is vital for developing efficient materials and enhancing electronic and chemical properties. Focusing on CsPbBr₃, we demonstrate a strategy for modifying electronic properties of lead halide perovskites through a systematic computational study on ligands with varying binding motif, size, bridge length, π -electron conjugation, and electron withdrawing and donating groups. The calculations are benchmarked against experimental data. Choosing a ligand's π -electron system and binding group, followed by tuning the ligand's properties with substituents to the π -system, allows one to introduce ligand electronic states into the perovskite system's bands, close to band edges, and inside the material's fundamental band gap. One can also design surface states by inducing local distortions at the binding site, which can be tuned by altering the binding group of the ligand. Extension of a material's frontier orbitals onto ligands and the creation of surface states makes charges available for transport and chemical reactivity, while avoiding charge trapping. In contrast, midgap ligand states trap charges permanently. Large ligands with high coverages interact among themselves, influencing ligand electronic properties and binding. Carboxylate tends to bind more strongly than the ammonium group. Electronegative oxygens in the carboxylate binding group and electron withdrawing substituents bound to the π -system lower ligand orbital energies relative to perovskite states. The reported theoretical analysis guides experimental design of perovskite-ligand systems for optoelectronic, energy and quantum information applications.

* Corresponding author. Email: prezhdo@usc.edu

TOC graphic



Metal halide perovskites, and more specifically lead halide perovskites (LHPs), have gained immense popularity in a wide array of optoelectronic applications including solar cells, light-emitting diodes (LEDs), detectors, and quantum information materials due to their excellent light absorption, high charge carrier mobility, and tunable bandgaps.^{1, 2} These materials are also relatively easy to synthesize and can be processed at low temperatures, making them cost-effective alternatives¹ to traditional silicon-based devices in large-scale manufacturing. Their potential for achieving high power conversion efficiencies (PCEs) coupled with their lightweight and adjustable nature opens up new avenues for innovative applications in solar cells and other electronic devices. As research on these cutting-edge materials advances, LHPs hold promise for revolutionizing renewable energy technologies with PCEs exceeding 26% reported as of 2024.³

The remarkable properties of LHPs have enhanced their PCEs to position them as legitimate competitors to traditional silicon-based solar cells. These properties can be tuned to fit a variety of uses, extending their applications past solar cells and into other areas such as in LED development and quantum information processes.^{4, 5} The composition and structure of LHPs can be fine-tuned through defect engineering,¹ doping and varying ligand compositions⁶ for precise control over their optical, chemical and electronic properties. Remarkably, defects in LHPs are not detrimental in applications, and LHPs can retain high efficiencies and desirable properties despite defect abundance and varied composition.⁷ By adjusting the compositional characteristics of LHPs, properties such as bandgap, charge transport, and color emission can be selectively modified.^{1, 6} Additionally, LHPs have low exciton binding energies⁸⁻¹⁰ which allow for effective separation of electron and hole. This separation introduces efficient charge transport and subsequently high efficiencies in optoelectronic applications. Lastly, these materials have strong absorption coefficients.⁸ LHPs can absorb a broad spectrum of wavelengths, an ideal property for solar cell applications. This combination of high performance, tunability, low-cost fabrication, and extensive versatility make LHPs a promising alternative to traditional semiconductor materials.

LHP quantum dots (QDs) have emerged as a fascinating class of nanomaterials due to their excellent optical properties including size-tunable photoluminescence and high quantum efficiency.^{2, 6, 11, 12} These properties make them attractive for LEDs,^{5, 6} lasers,^{10, 13} and photodetectors.² The ability to control the emission wavelength by simply altering the QD size allows for the development of highly efficient, color-pure sources of light.¹⁰ QD assemblies represent another advancement in nanotechnology and optoelectronics. Individual QDs are organized into larger structures with the goal to enhance their collective properties and functionalities.^{1, 14, 15} This strategy allows for the emergence of unique optical and electronic behaviors that differ from isolated QDs.^{14, 16} One can tune QD assemblies for specific applications by adjusting QD size, arrangement, spacing and coupling.^{10, 17-20} The self-assembly of QDs can be scaled for manufacturing purposes, similar to that of bulk LHP materials.

LHP QDs hold promise for quantum information technology^{2, 8, 21, 22} in which quantum mechanical properties are used to perform computations and transmit information in ways that classical systems cannot achieve. Quantum processes use quantum bits, or qubits, which exist in a superposition of states that can create avenues for parallel processing of information within the qubit.²² This can significantly increase the speed for certain classes of problems compared to traditional computers, and can provide answers for problems that are impossible to solve through traditional means.²² For example, quantum

computing has been shown to be an effective tool in areas such as cryptography²¹ and drug discovery.²³⁻²⁵ The high quantum efficiencies and narrow emission linewidths^{2, 26} of LHP QDs allow for precision control of light at the quantum level and their tunable bandgap creates opportunities for qubit design.²⁶ Lastly, LHP QDs can achieve long quantum coherence at low²⁷ and even room temperatures,⁸ an ideal characteristic for the practical application of quantum computing. Arranging LHP QDs into two- or three-dimensional networks and placing the systems into optical cavities^{28, 29} allows one to design and manipulate the coupling between QDs and their light emission properties.

In this letter, we consider a systematic set of ligands that can be used to passivate LHP QD surfaces and control inter-dot coupling in QD assemblies. We show that judicious ligand design can be used to extend QD wavefunctions onto ligands, thereby enhancing inter-dot interactions. On the other hand, some ligands can introduce midgap electronic states that trap charge carriers and quench QD emission, having a strong negative effect on QD electro-optic properties. The energetics of the ligand states relative to the LHP QD frontier orbitals depend on the extent of the ligand's π -conjugated system, the presence of electron withdrawing and donating substituents in the π -system, the binding group, and QD size. Larger π -electron conjugation lowers ligand excitation energies and brings ligand energy levels closer to the LHP QD band edges, with ligand contributions even found inside the bandgap in certain cases. The electronegative oxygen atoms in the carboxylate binding group lower ligand levels compared to the more positive ammonium binding group. Electron withdrawing substituents in a ligand's π -conjugated system also lower ligand energy levels, while electron donating groups raise the levels. Because of the quantum confinement effect, the positioning of the ligand levels relative to the QD frontier levels depends on QD size for sufficiently small QDs. For all considered ligands, only unoccupied energy levels can be brought close to the QD conduction band (CB) edge or inside the bandgap, while occupied levels of the ligands always remain deep inside the valence band (VB). Ligand binding energy calculations demonstrate that the carboxylate group binds as a bidentate ligand and tends to provide stronger binding than the ammonium group. An extra methylene group in the bridge allows for more flexibility and stronger binding. The calculated results are benchmarked against experimental data on photoluminescence (PL) quenching.

The study presented herein focuses on the all-inorganic CsPbBr₃ LHP, which is one of the most common choices for synthesizing LHP QDs. Ligand binding to CsPbBr₃ can occur through an ammonium cation at the A-site by replacement of a Cs cation, or through a carboxylate group by replacement of a bromide in the octahedral lead complex. Fifteen different ligands are selected for the study, fourteen of which contain π -conjugated systems, Figure 1. Two ligands (**I** and **II**) bind to CsPbBr₃ through a carboxylate group. Their comparison is designed to investigate the effects of π -conjugation. The remaining ligands bind through the ammonium cation. Among them, there are large ligands with extended π -conjugation (**III-V**), ligands with the same π -electron system and either electron withdrawing or donating groups (**VI-X**), similar ligands but with longer carbon bridges to bind to the LHP (**XI-XIV**), and a ligand with two electronegative nitrogen atoms embedded into the π -conjugated system (**XV**).

Systems containing qualitatively similar ligands to the ones studied in this work have been considered previously. They include ligands with both electron withdrawing and donating groups,^{17, 30} ligands with π -conjugation,^{5, 18, 19, 31-33} and ligands with carboxylate^{18, 19, 34} and ammonium⁴ groups at the

preferred binding sites. The various electron withdrawing and donating groups will lower or raise the ligand's lowest unoccupied molecular orbital (LUMO), respectively. Longer bridges can increase flexibility in the bonding, facilitating the process. Most experimental ligands contain inert aliphatic chains which are omitted during the calculations of the system's electronic properties, since the aliphatic chains have little influence on the alignment of the frontier electronic energy levels.

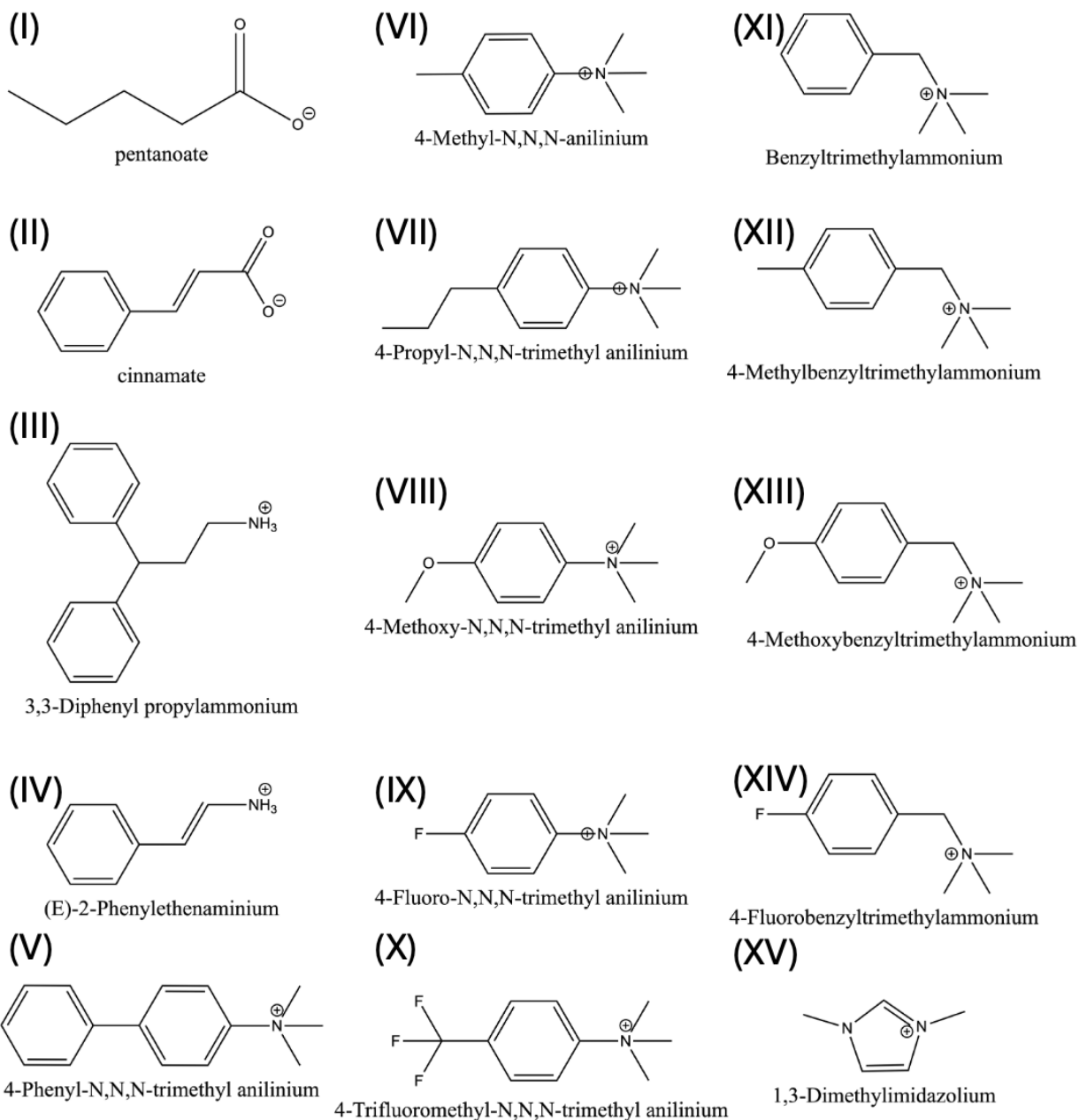


Figure 1. Ligand molecules considered. The binding motifs are illustrated in Figure 2, while the electronic properties are characterized in Figures 3-4 and S1-S5.

Selecting an accurate and efficient tool for calculating and characterizing the electronic properties of ligand-LHP systems is a challenging task. LHPs are periodic systems, while ligands are finite. LHPs exhibit significant screening of Coulomb interactions due to relatively large dielectric constants, and their exciton binding energies are relatively small. Thus, LHP electronic properties can be described reasonably well within the single-particle approximation, such as in the Kohn-Sham (KS) density functional theory (DFT). In comparison, an accurate description of electronic excitations in molecules typically require at least linear response (LR) DFT. LHPs contain heavy elements, in particular Pb, which exhibit strong spin-orbit coupling (SOC) effects, while SOC effects are insignificant in organic matter. Luckily, a fortuitous cancellation of various errors enables us to use the computationally efficient Perdew-Burke-Ernzerhof (PBE) functional.³⁵ In particular, the PBE functional is known to underestimate energy gaps in most semiconductors due to the electron self-interaction error. However, PBE produces good bandgap values for LHPs, because the self-interaction error and neglect of SOC cancel each other.³⁶ The energy gaps between the highest occupied molecular orbital (HOMO) and LUMO of the ligands calculated by PBE reproduce reasonably well the lowest electronic excitation energy of the types of molecules considered here. Thus, the excitation energy of benzene, ~ 4.9 eV,³⁷ can be well represented by the HOMO-LUMO gap obtained using the PBE functional. Even if the KS HOMO-LUMO gaps can accurately represent electronic excitations in the QD and ligand systems, this does not guarantee that the relative alignment of QD and ligand levels is correct. To investigate this, we report experimental PL data for the cinnamate ligand. The data confirms the existence of a midgap ligand state predicted by the PBE calculation. This is observed through PL quenching, a key aspect of midgap states. In addition to the PBE calculations, we also report PBE+SOC results, as well as results of calculations obtained with the hybrid Heyd-Scuseria-Ernzerhof³⁸ (HSE) functional, and HSE+SOC data. The electronic properties obtained with HSE are reported for PBE optimized geometries. It is important to stress that the reported results should be interpreted semi-quantitatively, and that trends rather than absolute values should be considered more beneficial for analysis.

The calculations in this work were performed with the Vienna Ab initio Simulation Package³⁹ (VASP). All structures were initially optimized using the PBE functional using 3x3x1 k-point mesh. The plane-wave basis energy cutoff was 520 eV and Grimme's DFT-D3 dispersion correction⁴⁰ was utilized. For the PBE single point calculations, a finer 5x5x1 k-point mesh was used. All other single point calculations (PBE+SOC, HSE, HSE+SOC) were carried out at the Γ -point only for computational efficiency. Both singlet and triplet calculations were performed. Because LHP QDs used in experiment are much larger than those accessible by ab initio simulation, the LHP is represented by a slab made with a 2x2x3 supercell with two exposed surfaces, once of which is used for ligand binding. The cubic phase CsPbBr₃ was used to construct the supercell slab. The slab was 3 layers thick with the (100) surface exposed for binding. The LHP primitive cell was taken from the Materials Project⁴¹ (ID: mp-600089). The ligand binding energies were calculated as:

$$E_{Ads}(eV) = (E_{Ligand+LHP} + E_{Cs/BrAtom}) - (E_{Ligand} + E_{LHP}) \quad (1)$$

Here, $E_{Ligand+LHP}$ is the energy of the ligand-LHP complex, $E_{Cs/BrAtom}$ is the energy of the cesium or bromine atom (which the ligand replaces upon binding), and E_{Ligand} and E_{LHP} are the energies of the ligand and LHP, respectively.

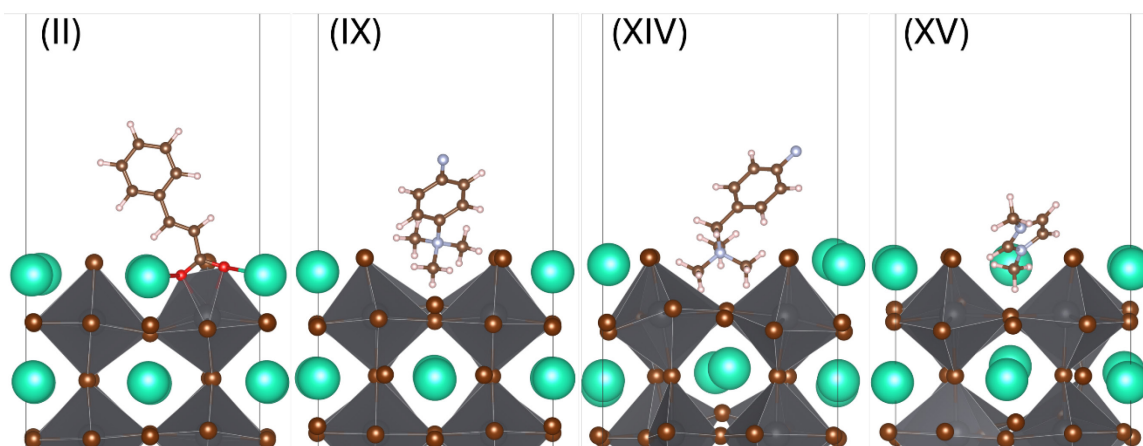


Figure 2. Ligand-LHP binding motifs illustrated through four distinct cases, exemplified by ligands **II**, **IX**, **XIV**, and **XV**, Figure 1. A cesium atom is removed for systems **IX**, **XIV**, and **XV** to better visualize their binding motifs.

Figures 2 and 3 illustrate the ligand binding motifs and LUMO charge densities, respectively, with four representative cases. The first case, ligand **II** containing a carboxylate group, binds through said group and replaces a bromine atom (representative of **I** and **II**). The second case, ligand **IX**, has a shorter chain connected to its ammonium group (ligands **III-X**), and the third case, represented by **XIV**, has a longer chain, allowing for more flexibility in binding to the LHP QD (ligands **XI-XIV**). Simultaneously, binding through these longer bridges leads to larger local distortions in the LHP QD. Lastly, the small **XV** ligand binds to the LHP without any bridge. Due to its size, this ligand barely extends past the LHP surface. Ligands **IX**, **XIV** and **XV** replace the A-site cesium cation.

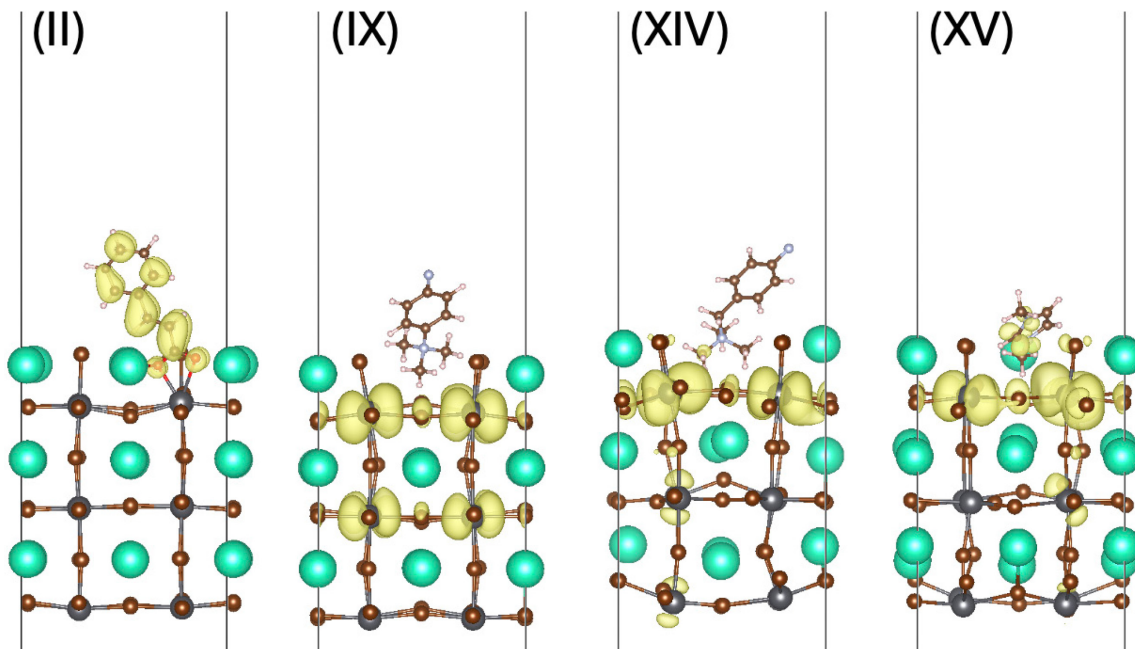


Figure 3. LUMO charge densities of the representative systems shown in Figure 2, obtained with the PBE functional. The LUMO of **II** is localized on the ligand. The LUMOs of **IX** and **XV** are localized on the LHP. The LUMO of **XIV** is delocalized between the ligand and the LHP. A cesium atom is removed for systems **IX** and **XIV** to better visualize their binding motifs. For similar reasons, the polyhedral formation of the LHP QD is not visualized to better observe the charge densities located within the QD structure (**IX**, **XIV**, **XV**).

Figure 3 demonstrates LUMO charge densities of the four representative systems discussed in Figure 2. Three different situations are encountered. The LUMO of system **II** is localized on the cinnamate ligand, suggesting that it can act as an electron trap. The LUMO is supported by the π -conjugated electronic system and extends onto the carboxylate binding group. The presence of electronegative atoms of the carboxylate group lowers the LUMO energy below the perovskite conduction band minimum (CBM), Figure 4. In comparison, the LUMO of the same ligand with the ammonium binding group, ligand **IV**, is slightly above the perovskite CBM. The LUMO of system **IX**, representing the shorter-bridge category of the investigated ligands, is delocalized across the LHP, with charge density distributed primarily over lead atoms, as well as their connecting bromine atoms.

The longer-bridge ligands, represented by ligand **XIV** in Figure 3, exhibit a more significant reconstruction of the binding site. This results in an increased localization of the LUMO on the LHP surface compared to the shorter-bridge ligands. In this example, the LUMO is still localized on the LHP as in the case with the shorter bridge (**IX**). However, the charge is drawn to the surface, which can favor interactions with charges photogenerated in the LHP with surface species and other QDs. It is important to note that the surface state observed with system **XIV**, Figure 3, is part of the LHP CB, Figure 4. Therefore, it does not trap charges permanently, and charges drawn to the LHP surface by the surface state can easily escape into bulk. The final system in Figure 3, containing ligand **XV**, exemplifies the situation,

in which the LUMO charge density is delocalized between the LHP and the ligand. Similar to the ligand **XIV** system, the charge migrates from within the LHP to the surface where the ligand binds, and the terminal bromine atom closest to the ligand gains charge density. The charge density also extends onto the electronegative nitrogen atoms of the ligand as well as the carbon atom separating them.

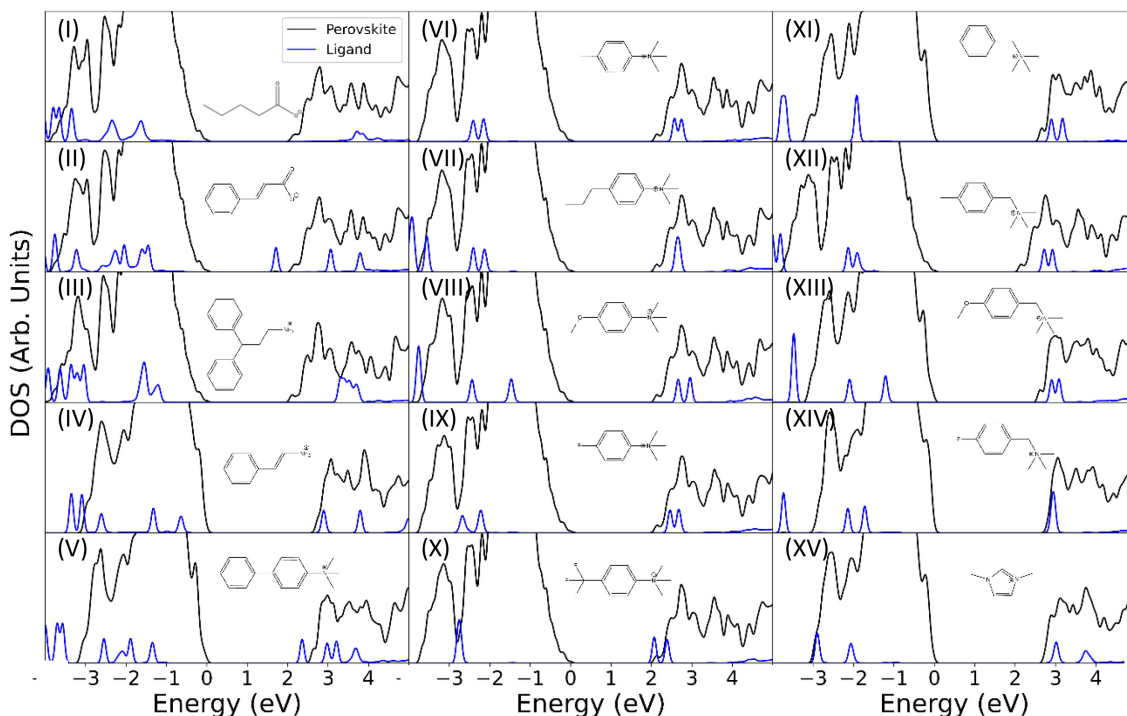


Figure 4. Densities of states (DOS) obtained with the PBE functional in the singlet state, and separated into ligand and perovskite contributions.

The energies of the ligand states relative to the LHP VB and CB are illustrated through plotting the density of states (DOS), Figure 4. The DOS are obtained with the PBE functional, which should present the most useful results, as discussed previously and supported by the experimental data in Figure 5. DOS plots obtained with other methods are shown in Figures S1-S5, including HSE in the singlet and triplet states, HSE+SOC, and PBE in the triplet state. Different approaches give different quantitative results, and therefore, it is more valuable to consider qualitative trends rather than absolute values.

For all of the systems, except **III**, the ligands contribute narrow peaks to the DOS. This is indicative of negligible interaction between periodic images of the ligands in the simulation. I.e., even at a high degree of ligand coverage, ligand states maintain their molecular identity and do not form bands. Ligand **III** is an exception due to its large size, making the π -electron systems of periodically replicated ligand molecules interact and form narrow bands.

Various trends can be observed from the DOS of the systems, including effects caused by the extent of π -electron conjugation, inclusion of electronegative elements as well as electron donating and withdrawing groups, and ligand bridge length. As the size of the π -conjugated system increases, e.g,

systems **II**, **IV**, **V**, the energy of the ligand LUMO decreases. In systems **II** and **V**, the energies of the ligand orbitals decrease significantly in the CB, potentially forming shallow electron trap states not present in the other ligands studied. The presence of more electronegative elements lowers the LUMO as well, which is seen when the carboxylate group containing two oxygens in **II** and the aminium group containing one nitrogen in **IV** are compared.

The effects of electron withdrawing versus donating groups is also illustrated in Figure 4. Fluorine is used as the electron withdrawing group in ligands **IX**, **X**, and **XIV**. The ether substituents in **VIII** and **XIII** are electron donating through resonance, while at the same time they exhibit an electron withdrawing inductive effect. The methyl groups in **VI** and **XII**, and the propyl group in **VII** act as electron donating groups. When electron withdrawing groups are added to the ligand, the ligand LUMO energies decrease, and in the case of ligand **X** which contains three electronegative fluorine atoms, drop below the LHP CBM. While the influence of the electron donating and withdrawing groups to the π -conjugated system has been studied for the ligands with the ammonium binding group, similar conclusions can be expected for carboxylate ligands. These observations provide key insights into how electron withdrawing and donating groups can be used to tune the electronic structure of the ligand-LHP QD systems.

Additional DOS plots are included in the Supporting Information (SI). The DOS was additionally calculated with SOC for both the PBE and HSE functionals, as well as for both singlet and triplet spin states without SOC. Figure S1 shows the DOS calculated with the HSE functional in the singlet state. There is a distinct increase of the band gap, by ~ 1 eV in some cases, e.g., **IV** and **V**. The HSE and HSE+SOC DOS are calculated only at the Γ k-point. For this reason, the DOS shown in Figures S1, S2, S4, S5 exhibit sharp peaks in the LHP component. Incorporating SOC decreases the LHP band gap, Figure S2. At the same time, the energy levels of the ligands change little upon including SOC. In particular, the energy of the cinnamate (ligand **II**) LUMO is significantly above the LHP CBM in the HSE+SOC calculation in Figure S2. This contradicts the experimental results discussed below and visualized in Figure 5. The triplet state PBE DOS in Figure S3 shows a slight splitting in some of the ligands' DOS, including systems **II**, **X**, and **V**, listed from most pronounced to least pronounced splitting. In the case of **II**, the shallow trap state shown in Figure 4 is realized only in one spin direction in Figure S3. On the other hand, the shallow trap state in **V** in Figure 4 disappears when the triplet state DOS is considered. In a few of the ligand systems studied, the HSE calculation for the triplet state exhibits midgap states that can act as charge traps, Figure S4.

It is also of interest to investigate the adsorption energies of the ligand-LHP systems. The adsorption energy describes the strength, preference, and likelihood of the ligand binding to the LHP QD. The more negative the adsorption energy, the more likely the ligand is to bind. Adsorption energies were computed for all ligand-LHP systems using Eq. (1). The results are then summarized in Table 1. Ligands **I** and **II**, which bind to the LHP through the carboxylate group, show large negative adsorption energies, indicating a strong binding to the LHP. Ligand **XV**, the smallest ligand, exhibits one of the weakest adsorptions. This is consistent with the shape of the ligand and the binding motif in Figure 2. The ligand does not contain a tail as in the other examples, thereby promoting steric hindrance as the ligand cannot bind to the LHP in an effective way. The less favorable adsorption energy is exacerbated by the nitrogen atoms lying within the π -conjugated ring and therefore at suboptimal positions for binding compared to

the systems that have ammonium ions at terminal or branched points (**III-XIV**). The LHP QD system containing ligand **X** also has a characteristically high adsorption energy. The presence of three strongly electron withdrawing fluorine atoms in **X** is likely the cause of its less favorable adsorption. Ligand **III** exhibits the strongest absorption, likely because of its large size, allowing for ligand-ligand interactions at high ligand coverage, stabilizing the ligand-LHP system.

Table 1. The adsorption energies of the systems studied. The ligand numbering matches that of Figure 1.

| System | Adsorption Energy (eV) |
|--------|------------------------|
| I | -1.813 |
| II | -1.825 |
| III | -1.918 |
| IV | -1.450 |
| V | -1.491 |
| VI | -1.465 |
| VII | -1.483 |
| VIII | -1.536 |
| IX | -1.471 |
| X | -1.270 |
| XI | -1.658 |
| XII | -1.481 |
| XIII | -1.839 |
| XIV | -1.577 |
| XV | -1.339 |

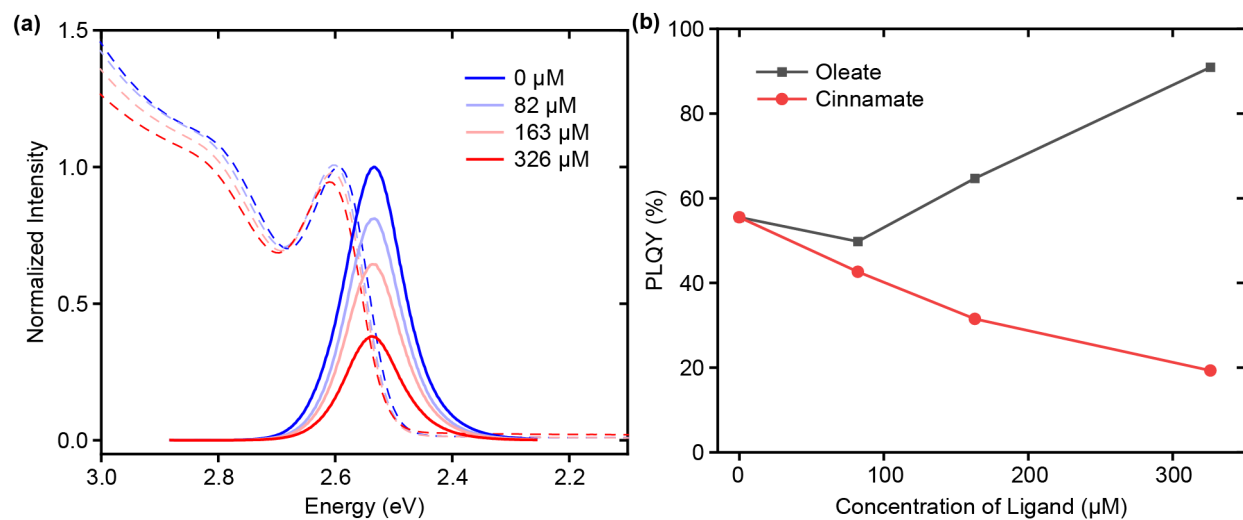


Figure 5. (a) UV-Vis and PL spectra for CsPbBr₃ quantum dots with added cinnamate ligand at varying concentration. (b) PLQY of CsPbBr₃ quantum dots with added cinnamate or oleate ligand.

In order to provide an experimental verification of the reported calculations, and differentiate between the various DOS calculations that give qualitatively different results, experimental studies were performed with the cinnamate (**II**) ligand, as summarized in Figure 5. The experimental methods are described in the SI. Figure 5a reports both UV-Vis and photoluminescence (PL) spectra for the cinnamate-LHP QD system with varying ligand concentrations. As the concentration increases, the PL intensity decreases, indicating that cinnamate creates a trap state that quenches PL. This experimentally observed trap state is consistent with the predicted DOS using the PBE functional as shown in Figure 4. In comparison, both the HSE and HSE+SOC calculations, Figures S1 and S2, respectively, do not show ligand states inside the LHP band gap. The experimental data confirms that the PBE level of theory provides more reliable results. The UV-Vis and PL spectra of the ligand-LHP QD system qualitatively similar to ligand **I** can be found in Figure S6. Oleate is an aliphatic hydrocarbon containing no π -conjugation. Its HOMO and LUMO orbitals are widely separated in energy (as illustrated in the DOS calculations), and none of the calculations predict midgap states for oleate. The experimental data show that the PL intensity increases with increased oleate concentration, likely due to better passivation of intrinsic defects on LHP surface. The dependence of the PL quantum yield on ligand concentration for cinnamate and oleate ligands is compared in Figure 5b, confirming the above conclusions. Lastly, Figure S6 contains additional analysis showing an average nanoparticle size of 5.4 nm. Particles of this size contain many thousands of atoms, extending beyond capabilities of current ab initio electronic structure methods, justifying the slab model used in the present studies.

In conclusion, we have screened fifteen different ligands, elucidating their binding motifs and influence on the electronic properties of the bound ligand-LHP QD systems. Various ligand characteristics have been studied, including extent of the π -electron conjugated system, electron withdrawing and donating groups, ligand size, bridge length, and binding type. Several levels of electronic structure calculations have been considered and benchmarked with experimental measurements. Comparison with experiment has indicated that the simple PBE level of theory provides the best results due to fortuitous cancelation of several systematic errors. The more advanced HSE functional and inclusion of SOC effects make the calculations less reliable overall at an increased computational expense, further supporting the preference of the PBE functional for accurate calculations. The calculations reveal several important trends that can guide design of LHP ligands. The carboxylate group tends to provide stronger binding than ammonium because it acts as a bidentate ligand. The electronegative oxygen atoms present in the carboxylate group lower orbital energy levels of the ligand compared to the ammonium binding group. Ligand binding can induce notable local distortions in the LHP around the binding site (most clearly observed in ligands containing large bridges), and the distortion tends to increase the local LHP band gap. It is possible to design ligands with electronic state energies located inside the LHP bands, close to the CB edge, and inside the fundamental band gap. None of the considered ligands exhibited states near the VB edge. The energy of the ligand LUMO can be lowered by increasing the size of the ligand's π -electron conjugated system and through introducing electronegative, electron withdrawing atoms and substituents. One can easily obtain systems with frontier orbitals localized on either the LHP or ligand. More careful design is needed to have frontier orbitals extend between the LHP and ligands. Extension of LHP electronic states onto ligands promotes interactions between LHP QDs and makes charges more

readily available for transport and chemical reactivity. One can also design ligands that localize frontier orbitals onto the LHP surface without extending said orbitals onto the ligands. This occurs through local surface distortions at the binding site. Such surface states do not act as charge traps. Charges can easily escape into the LHP bulk, while at the same time they are available on the surface to perform chemical reactions or participate in charge or exciton transport. At high ligand coverage and with large ligands, ligand-ligand interactions can become important, influencing ligand binding and electronic properties. A general strategy for design of ligand-LHP systems can be suggested by first considering a combination of the π -electron conjugated system and binding group, and then fine-tuning the ligands' electronic energy levels by electron withdrawing or donating substituents to the π -system. The trends found with ligands to the CsPbBr₃ perovskite should be applicable generally to other metal halide perovskites as well. The reported results provide important guidelines and insights into ligand design for LHP applications in photovoltaics, optoelectronics, quantum information systems, and beyond.

Acknowledgements.

The research was supported by the US National Science Foundation through the DMREF program (grant #2324299). This work was supported in part by the Research Instrumentation Center in the Department of Chemistry at Purdue University. Electron microscopy was performed using instrumentation in the Purdue Electron Microscopy Center (RRID:SCR_022687).

Supporting Information.

Experimental methods. Projected densities of states obtained with other functionals.

References.

- (1) Kovalenko, M. V.; Protesescu, L.; Bodnarchuk, M. I., Properties and Potential Optoelectronic Applications of Lead Halide Perovskite Nanocrystals. *Science* **2017**, *358*, 745-750.
- (2) Peighambardoust, N. S.; Sadeghi, E.; Aydemir, U., Lead Halide Perovskite Quantum Dots for Photovoltaics and Photocatalysis: A Review. *ACS Applied Nano Materials* **2022**, *5*, 14092-14132.
- (3) Shen, Y.; Zhang, T.; Xu, G.; Steele, J. A.; Chen, X.; Chen, W.; Zheng, G.; Li, J.; Guo, B.; Yang, H.; Wu, Y.; Lin, X.; Alshahrani, T.; Yin, W.; Zhu, J.; Wang, F.; Amassian, A.; Gao, X.; Zhang, X.; Gao, F.; Li, Y.; Li, Y., Strain Regulation Retards Natural Operation Decay of Perovskite Solar Cells. *Nature* **2024**, *635*, 882-889.
- (4) Li, N.; Apergi, S.; Chan, C. C. S.; Jia, Y.; Xie, F.; Liang, Q.; Li, G.; Wong, K. S.; Brocks, G.; Tao, S.; Zhao, N., Diammonium-Mediated Perovskite Film Formation for High-Luminescence Red Perovskite Light-Emitting Diodes. *Advanced Materials* **2022**, *34*, 2202042.
- (5) Wang, H.; Ye, F.; Sun, J.; Wang, Z.; Zhang, C.; Qian, J.; Zhang, X.; Choy, W. C. H.; Sun, X. W.; Wang, K.; Zhao, W., Efficient CsPbBr₃ Nanoplatelet-Based Blue Light-Emitting Diodes Enabled by Engineered Surface Ligands. *ACS Energy Letters* **2022**, *7*, 1137-1145.
- (6) Fiuza-Maneiro, N.; Sun, K.; López-Fernández, I.; Gómez-Graña, S.; Müller-Buschbaum, P.; Polavarapu, L., Ligand Chemistry of Inorganic Lead Halide Perovskite Nanocrystals. *ACS Energy Letters* **2023**, *8*, 1152-1191.
- (7) Mosquera-Lois, I.; Huang, Y.-T.; Lohan, H.; Ye, J.; Walsh, A.; Hoye, R. L. Z., Multifaceted Nature of Defect Tolerance in Halide Perovskites and Emerging Semiconductors. *Nature Reviews Chemistry* **2025**, Apr 7. doi: 10.1038/s41570-025-00702-w. Epub ahead of print.

- (8) Ricci, F.; Mandal, H.; Wajahath, M.; Burdick, R. K.; Villabona-Monsalve, J. P.; Hussain, S.; Goodson, T., III, Investigations of Coherence in Perovskite Quantum Dots with Classical and Quantum Light. *The Journal of Physical Chemistry C* **2023**, *127*, 3579-3593.
- (9) Gao, K.; Li, Y.; Yang, Y.; Liu, Y.; Liu, M.; Liang, W.; Zhang, B.; Wang, L.; Zhu, J.; Wu, K., Manipulating Coherent Exciton Dynamics in CsPbI₃ Perovskite Quantum Dots Using Magnetic Field. *Advanced Materials* **2024**, *36*, 2309420.
- (10) Zhu, C.; Boehme, S. C.; Feld, L. G.; Moskalenko, A.; Dirin, D. N.; Mahrt, R. F.; Stöferle, T.; Bodnarchuk, M. I.; Efros, A. L.; Sercel, P. C.; Kovalenko, M. V.; Rainò, G., Single-Photon Superradiance in Individual Caesium Lead Halide Quantum Dots. *Nature* **2024**, *626*, 535-541.
- (11) Ghosh, A.; Mora Perez, C.; Brosseau, P.; Dirin, D. N.; Prezhdo, O. V.; Kovalenko, M. V.; Kambhampati, P., Coherent Multidimensional Spectroscopy Reveals Hot Exciton Cooling Landscapes in CsPbBr₃ Quantum Dots. *ACS Nano* **2025**, *19*, 14499-14508.
- (12) Ran, J.; Wang, B.; Wu, Y.; Liu, D.; Mora Perez, C.; Vasenko, A. S.; Prezhdo, O. V., Halide Vacancies Create No Charge Traps on Lead Halide Perovskite Surfaces but Can Generate Deep Traps in the Bulk. *The Journal of Physical Chemistry Letters* **2023**, *14*, 6028-6036.
- (13) Zhong, H.; Yu, Y.; Zheng, Z.; Ding, Z.; Zhao, X.; Yang, J.; Wei, Y.; Chen, Y.; Yu, S., Ultra-Low Threshold Continuous-Wave Quantum Dot Mini-Bic Lasers. *Light: Science & Applications* **2023**, *12*, 100.
- (14) Ye, J.; Gaur, D.; Mi, C.; Chen, Z.; Fernández, I. L.; Zhao, H.; Dong, Y.; Polavarapu, L.; Hoye, R. L. Z., Strongly-Confined Colloidal Lead-Halide Perovskite Quantum Dots: From Synthesis to Applications. *Chemical Society Reviews* **2024**, *53*, 8095-8122.
- (15) Chistyakov, A. A.; Zvaigzne, M. A.; Nikitenko, V. R.; Tameev, A. R.; Martynov, I. L.; Prezhdo, O. V., Optoelectronic Properties of Semiconductor Quantum Dot Solids for Photovoltaic Applications. *The Journal of Physical Chemistry Letters* **2017**, *8*, 4129-4139.
- (16) Mortemousse, P.-A.; Chanrion, E.; Jadot, B.; Flentje, H.; Ludwig, A.; Wieck, A. D.; Urdampilleta, M.; Bäuerle, C.; Meunier, T., Coherent Control of Individual Electron Spins in a Two-Dimensional Quantum Dot Array. *Nature Nanotechnology* **2021**, *16*, 296-301.
- (17) Zhang, B.; Goldoni, L.; Lambruschini, C.; Moni, L.; Imran, M.; Pianetti, A.; Pinchetti, V.; Brovelli, S.; De Trizio, L.; Manna, L., Stable and Size Tunable CsPbBr₃ Nanocrystals Synthesized with Oleylphosphonic Acid. *Nano Letters* **2020**, *20*, 8847-8853.
- (18) Vickers, E. T.; Graham, T. A.; Chowdhury, A. H.; Bahrami, B.; Dreskin, B. W.; Lindley, S.; Naghadeh, S. B.; Qiao, Q.; Zhang, J. Z., Improving Charge Carrier Delocalization in Perovskite Quantum Dots by Surface Passivation with Conductive Aromatic Ligands. *ACS Energy Letters* **2018**, *3*, 2931-2939.
- (19) Vickers, E. T.; Enlow, E. E.; Delmas, W. G.; DiBenedetto, A. C.; Chowdhury, A. H.; Bahrami, B.; Dreskin, B. W.; Graham, T. A.; Hernandez, I. N.; Carter, S. A.; Ghosh, S.; Qiao, Q.; Zhang, J. Z., Enhancing Charge Carrier Delocalization in Perovskite Quantum Dot Solids with Energetically Aligned Conjugated Capping Ligands. *ACS Energy Letters* **2020**, *5*, 817-825.
- (20) Chaban, V. V.; Prezhdo, V. V.; Prezhdo, O. V., Covalent Linking Greatly Enhances Photoinduced Electron Transfer in Fullerene-Quantum Dot Nanocomposites: Time-Domain Ab Initio Study. *The Journal of Physical Chemistry Letters* **2013**, *4*, 1-6.
- (21) Bozzio, M.; Vyvlecka, M.; Cosacchi, M.; Nawrath, C.; Seidelmann, T.; Loredò, J. C.; Portalupi, S. L.; Axt, V. M.; Michler, P.; Walther, P., Enhancing Quantum Cryptography with Quantum Dot Single-Photon Sources. *npj Quantum Information* **2022**, *8*, 104.
- (22) Wasielewski, M. R.; Forbes, M. D. E.; Frank, N. L.; Kowalski, K.; Scholes, G. D.; Yuen-Zhou, J.; Baldo, M. A.; Freedman, D. E.; Goldsmith, R. H.; Goodson, T.; Kirk, M. L.; McCusker, J. K.;

- Ogilvie, J. P.; Shultz, D. A.; Stoll, S.; Whaley, K. B., Exploiting Chemistry and Molecular Systems for Quantum Information Science. *Nature Reviews Chemistry* **2020**, *4*, 490-504.
- (23) Kumar, G.; Yadav, S.; Mukherjee, A.; Hassija, V.; Guizani, M., Recent Advances in Quantum Computing for Drug Discovery and Development. *IEEE Access* **2024**, *12*, 64491-64509.
- (24) Bikku, T.; Malligunta, K. K.; Thota, S.; Surapaneni, P. P., Improved Quantum Algorithm: A Crucial Stepping Stone in Quantum-Powered Drug Discovery. *Journal of Electronic Materials* **2025**, *54*, 3434-3443.
- (25) Santagati, R.; Aspuru-Guzik, A.; Babbush, R.; Degroote, M.; González, L.; Kyoseva, E.; Moll, N.; Oppel, M.; Parrish, R. M.; Rubin, N. C.; Streif, M.; Tautermann, C. S.; Weiss, H.; Wiebe, N.; Utschig-Utschig, C., Drug Design on Quantum Computers. *Nature Physics* **2024**, *20*, 549-557.
- (26) Jayan K, D.; Babu, K., Luminescent Perovskite Quantum Dots: Progress in Fabrication, Modelling and Machine Learning Approaches for Advanced Photonic and Quantum Computing Applications. *Journal of Luminescence* **2025**, *277*, 120906.
- (27) Utzat, H.; Sun, W.; Kaplan, A. E. K.; Krieg, F.; Ginterseder, M.; Spokoyny, B.; Klein, N. D.; Shulenberger, K. E.; Perkinson, C. F.; Kovalenko, M. V.; Bawendi, M. G., Coherent Single-Photon Emission from Colloidal Lead Halide Perovskite Quantum Dots. *Science* **2019**, *363*, 1068-1072.
- (28) Hu, Y.; Mao, D.; Chen, L.; Guan, Y.; Zhang, L.; Dong, H.; Xu, H.; Xie, W.; Sun, Z., Cavity-Enhanced Superfluorescence Stimulates Coherent Energy Transfer in a Perovskite Quantum Dot Superlattice. *Laser & Photonics Reviews* **2024**, *18*, 2400650.
- (29) Farrow, T.; Dhawan, A. R.; Marshall, A. R.; Ghorbal, A.; Son, W.; Snaith, H. J.; Smith, J. M.; Taylor, R. A., Ultranarrow Line Width Room-Temperature Single-Photon Source from Perovskite Quantum Dot Embedded in Optical Microcavity. *Nano Letters* **2023**, *23*, 10667-10673.
- (30) Zhang, Q.; Jiang, M.; Yan, G.; Feng, Y.; Zhang, B., Surface Ligand Engineering Involving Fluorophenethyl Ammonium for Stable and Strong Emission CsPbBr₃ Quantum Dots and High-Performance QLEDs. *Journal of Materials Chemistry C* **2022**, *10*, 5849-5855.
- (31) Frederick, M. T.; Weiss, E. A., Relaxation of Exciton Confinement in CdSe Quantum Dots by Modification with a Conjugated Dithiocarbamate Ligand. *ACS Nano* **2010**, *4*, 3195-3200.
- (32) Westmoreland, D. E.; López-Arteaga, R.; Kantt, L. P.; Wasielewski, M. R.; Weiss, E. A., Dynamic Tuning of the Bandgap of CdSe Quantum Dots through Redox-Active Exciton-Delocalizing N-Heterocyclic Carbene Ligands. *Journal of the American Chemical Society* **2022**, *144*, 4300-4304.
- (33) Westmoreland, D. E.; López-Arteaga, R.; Weiss, E. A., N-Heterocyclic Carbenes as Reversible Exciton-Delocalizing Ligands for Photoluminescent Quantum Dots. *Journal of the American Chemical Society* **2020**, *142*, 2690-2696.
- (34) Dutt, V. G. V.; Akhil, S.; Singh, R.; Palabathuni, M.; Mishra, N., Year-Long Stability and near-Unity Photoluminescence Quantum Yield of CsPbBr₃ Perovskite Nanocrystals by Benzoic Acid Post-Treatment. *The Journal of Physical Chemistry C* **2022**, *126*, 9502-9508.
- (35) Perdew, J. P.; Burke, K.; Ernzerhof, M., Generalized Gradient Approximation Made Simple. *Physical Review Letters* **1996**, *77*, 3865-3868.
- (36) Meggiolaro, D.; De Angelis, F., First-Principles Modeling of Defects in Lead Halide Perovskites: Best Practices and Open Issues. *ACS Energy Letters* **2018**, *3*, 2206-2222.
- (37) Kolos, W. o., Excitation Energies of Benzene. *The Journal of Chemical Physics* **1957**, *27*, 592-592.
- (38) Heyd, J.; Scuseria, G. E.; Ernzerhof, M., Hybrid Functionals Based on a Screened Coulomb Potential. *The Journal of Chemical Physics* **2003**, *118*, 8207-8215.
- (39) Kresse, G.; Hafner, J., Ab Initio Molecular Dynamics for Liquid Metals. *Physical Review B* **1993**, *47*, 558-561.

(40) Grimme, S.; Antony, J.; Ehrlich, S.; Krieg, H., A Consistent and Accurate Ab Initio Parametrization of Density Functional Dispersion Correction (Dft-D) for the 94 Elements H-Pu. *The Journal of Chemical Physics* **2010**, *132*, 154104.

(41) Jain, A.; Ong, S. P.; Hautier, G.; Chen, W.; Richards, W. D.; Dacek, S.; Cholia, S.; Gunter, D.; Skinner, D.; Ceder, G.; Persson, K. A., Commentary: The Materials Project: A Materials Genome Approach to Accelerating Materials Innovation. *APL Materials* **2013**, *1*, 011002.